Characterizing the Diurnal Cycle of Low-Level Circulation and Convergence Using CFSR Data in Southeastern South America

HENRIQUE FUCHS BUENO REPINALDO

Centro de Investigaciones del Mar y la Atmósfera, and Consejo Nacional de Investigaciones Científicas y Técnicas, Universidad de Buenos Aires, and Unidad Mixta Internacional: Instituto Franco–Argentino sobre Estudios de Clima y sus Impactos, Ciudad Universitaria, Buenos Aires, Argentina

MATILDE NICOLINI

Centro de Investigaciones del Mar y la Atmósfera, and Consejo Nacional de Investigaciones Científicas y Técnicas, Universidad de Buenos Aires, and Unidad Mixta Internacional: Instituto Franco–Argentino sobre Estudios de Clima y sus Impactos, and Departamento de Ciencias de la Atmósfera y los Océanos, Facultad de Ciencias Exactas y Naturales, Universidad de Buenos Aires, Ciudad Universitaria, Buenos Aires, Argentina

YANINA GARCÍA SKABAR

Unidad Mixta Internacional: Instituto Franco–Argentino sobre Estudios de Clima y sus Impactos, Ciudad Universitaria, and Servicio Meteorológico Nacional and Consejo Nacional de Investigaciones Científicas y Técnicas, Buenos Aires, Argentina

(Manuscript received 30 April 2014, in final form 15 November 2014)

ABSTRACT

The focus of this study is the characterization of the diurnal cycle of low-level wind and divergence field (under two different synoptic situations observed during the South American Low-Level Jet Experiment) within the South American domain encompassed between 20° and 35°S east of the Andes, using Climate Forecast System Reanalysis (CFSR). The objective is to highlight the existence of a spatial variation of these quantities and differences in the strength of their diurnal cycle between the two synoptic situations. Inertial oscillations and thermally driven circulations as well as convection-related contributions to mesoscale convergence and their implications for deep convection initiation/maintenance are addressed in each selected subregion. Prevalence of synoptic-scale forcing over the diurnally forced circulations, or vice versa, is also analyzed. Both mesoscale wind diurnal cycle and related divergence fields are sensitive to varying synoptic conditions and display regional variability. Thermal circulations related to topographical features superpose on the diurnal inertial oscillation that, while present in the whole domain, dominates the central plain subregions. The most evident diurnal cycle in the divergence field is restricted to sloped areas just to the east of the Andes and the Sierras de Córdoba where the mesoscale component of the divergence field is responsible for modulating the total divergence. CFSR provides a broad perspective of low-level circulation over southeastern South America (SESA) during the specific 15-day period. Results from this study might stimulate future research on a relationship between low-level circulation and the initiation of convection in SESA using CFSR to perform high-resolution simulations.

1. Introduction

Convergence zones originated by orography-related mesoscale circulations, land–sea discontinuities, and surface *inhomogeneities* favor the generation of moist convection (Szoke et al. 1984; Wilson and Schreiber 1986; Segal et al. 1989; Wilson et al. 1992; Pielke 2001; Wilson and Roberts 2006). Knowing the orographic mechanisms that drive the initiation and intensification of deep convection is important for forecasting purposes. Those mechanisms include forced ascent of flow upstream and downstream of moderate-height mountains, blocked flow, the formation of convergence areas within flow modified by orography, differential warming, and leeward waves (Tripoli and Cotton 1989a,b; Banta 1990; Wolyn and McKee 1994; Romatschke and Houze 2010; Houze 2012).

Corresponding author address: Henrique Fuchs Bueno Repinaldo, Centro de Investigaciones del Mar y la Atmósfera, CONICET, Universidad de Buenos Aires, Pab. 2, 2°Piso, Ciudad Universitaria, C1428EGA, Ciudad Autónoma de Buenos Aires, Argentina.
E-mail: hrepinaldo@cima.fcen.uba.ar

DOI: 10.1175/JAMC-D-14-0114.1

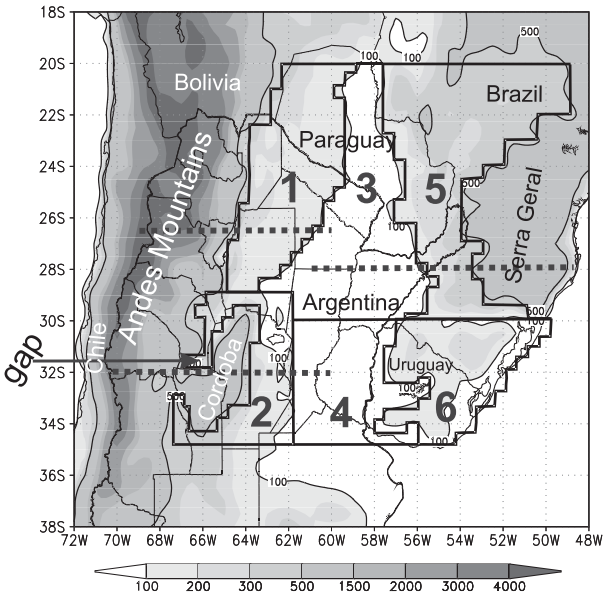

FIG. 1. Study domain. Subregions outlined with heavy lines were used to calculate the averages of the analyzed variables. Gray shading indicates the topography in meters (scale at the bottom). The dashed lines are the locations for the cross-sectional plots in Fig. 5. The arrow indicates the position of the "gap" mentioned in the text.

Southeastern South America (SESA) mostly encompasses continental latitudes to the east of the Andes between 20° and 35°S (Fig. 1). The region is characterized by the Andes, lower elevations immediately to the east of the Andes, Sierras de Córdoba, and Serra Geral on the coast of the Atlantic Ocean in Brazil. SESA is known for being one of the two regions in the world where the most intense mesoscale convective systems (MCSs) occur (Zipser et al. 2006). A large number of these convective systems develop in the presence of a low-level jet (Conforte 1997; Torres 2003). The jet is called the South American low-level jet (SALLJ) and provides the dynamic and thermodynamic conditions that favor the transport of moisture from the Amazon basin (Berri and Inzunza 1993; Douglas et al. 1998; Paegle 1998; Saulo et al. 2000; Nieto Ferreira et al. 2003; Marengo et al. 2004; Salio et al. 2007) and the development of convection over SESA (Velasco and Fritsch 1987; Nicolini et al. 2002; Salio et al. 2002; Nicolini and Saulo 2006; Romatschke and Houze 2010). The Variability of the American Monsoon Systems (VAMOS) program (CLIVAR/WCRP) developed a SALLJ project aimed at understanding the role of SALLJ in moisture and energy exchange between the tropics and extratropics and carried out a field campaign, the South American Low-Level Jet Experiment (SALLJEX; Vera et al. 2006), between 15 November 2002 and 15 February 2003. An upper-air network, including radiosonde and pilot balloon sites, was established during SALLJEX to reduce the upper-air observational gaps existing in the region. Special in situ measurements were made in Bolivia, Paraguay, central and northern Argentina, and western Brazil.

Diurnal oscillation of the low-level ageostrophic wind component is one of the mechanisms proposed to explain the low-level jet formation. According to the theory proposed by Blackadar (1957), during surface radiative warming winds near the top of the boundary layer tend to be subgeostrophic through turbulent momentum transport as the surface layer is coupled with the boundary layer and a balance of forces is achieved that includes friction. Radiative cooling at night stabilizes the near-surface layer, turbulent vertical mixing is reduced, and the winds in the residual layer become decoupled from the shallow surface layer and consequently from the effects of friction. The lack of friction in the upper portion of the shallow nocturnal boundary layer results in an imbalance of forces. Wind accelerates because of the synoptic pressure gradient and the Coriolis force induces an inertial oscillation of the wind that gives rise to supergeostrophic winds at night. Bonner and Paegle (1970), Arritt et al. (1997), and Whiteman et al. (1997), among others, have documented diurnal variations in boundary layer winds over the south-central United States related to the inertial oscillation and to the diurnal oscillation of the horizontal pressure gradient over sloping terrain. In South America, Saulo et al. (2000) characterized the South American low-level flow during a spring–summer season using the regional Eta Model. The summer mean diurnal wind gyre at 900 hPa displays a strong diurnal cycle that determines a backing of the anomalies consistent with Blackadar's concept. Also, downslope winds at night (between 0600 and 1200 UTC) and upslope winds (between 1800 and 0000 UTC) are detected in the model characterization. Nicolini et al. (2004) produced maps and hodographs of observed winds for different hours of the day during SALLJEX. They found an counterclockwise wind gyre at low levels during nocturnal time consistent with an inertial oscillation stronger at subtropical latitudes and an opposite rotation during daytime with an easterly component at nightfall toward low pressure. This opposite rotation accompanies in time the deepening of a thermal–orographic low pressure system close to the Andes, known as the northwestern Argentina low (NAL; Seluchi et al. 2003). Maximum and minimum northerly winds are observed between 0600 and 1200 UTC and 1800 and 0000 UTC, respectively. Hodographs of the wind anomaly with respect to the daily mean describe an counterclockwise rotation during the whole day. This behavior is more clear in composites obtained during intensive observing periods and strong SALLJ events.

The relationship between the onset of convective systems and mesoscale circulations is poorly studied in the SESA region. Romatschke and Houze (2010) using Precipitation Radar (PR) data from the Tropical Rainfall Measuring Mission (TRMM; Kummerow et al. 1998) found that during the evening and the night there was an increase in the number of deep convective radar echo structures east of the Andes, which might be related to the convergence phase of the diurnal cycle of the wind. García Skabar and Nicolini (2009) generated a set of enriched analyses using the Brazilian Regional Atmospheric Modeling System (BRAMS; Cotton et al. 2003; Freitas et al. 2009) with spatial resolution of 20 km (hereinafter BRAMS-20), assimilating data obtained during SALLJEX.

Using the BRAMS-20 analyses, Nicolini and García Skabar (2011, hereinafter NGS) examined the existence of mesoscale flow and the diurnal cycle of divergence in SESA, which might force convection onset. They focused on the broad valley located between 50° and 70°W and between 20° and 35°S for a 15-day period during summer 2003, coincident with the SALLJEX warm season. Using BRAMS-20, evidence of a diurnal cycle on the mean circulation and divergence on the boundary layer were evaluated, taking into account two days within a period characterized by two different synoptic patterns. Total divergence (daily mean plus anomaly), total zonal divergence, and total meridional divergence were analyzed to explore a possible zonal effect associated with a northwest mountains–central plain mesoscale flow regime due to the main orientation north–south of the Andes and Sierras de Córdoba. According to breeze theories a nocturnal anomalous convergence and a diurnal anomalous divergence are expected. The authors found a diurnal cycle in the total divergence field in the boundary layer over the plains (as an average over the whole domain and over the 15-day-long period), with nocturnal convergence and daytime divergence. Daytime divergence is completely dominated by the zonal component while nocturnal convergence responds to the meridional component. Such total convergence attains its maximum at night, like maxima of precipitation and convection over Argentina that are also nocturnal (Nicolini and Saulo 2006; Salio et al. 2007; Monaghan et al. 2010). They found that this signal is also present in the entire warm-season (SALLJEX) period. They concluded that the diurnal cycle of the boundary layer divergence is not a peculiar feature related to the particular synoptic situations included in the analysis but a common characteristic at least during the warm season.

NGS results show convergence and divergence maxima concentrated close to the Andes and Sierras de Córdoba indicating a distance of orographic effect in divergence patterns. These results motivated the interest in subdividing the study domain in subregions to differentiate those with gentle slopes close to the Andes, the plains in the middle of the region, and the areas with a smooth slope at the east near to Serra Geral in Brazil and to the Atlantic coast.

In the present paper that uses the Climate Forecast System Reanalysis analysis (CFSR), the following questions that were not addressed by NGS are posed:

1) Is there significant spatial variation in the strength of diurnally forced circulations and of their related divergences considering the selected subregions?
2) Under what synoptic conditions are the amplitudes of the average low-level diurnal wind oscillation—as an estimate of the strength of the diurnal forcing of the wind field—in each subregion stronger and why?
3) During what synoptic conditions is the diurnal cycle of low-level mesoscale convergence stronger? Is this result conditioned by the presence of rainfall related to large precipitating MCSs that span the study domain?
4) Which diurnal cycle of deep moist convection would be expected in the different subregions in terms of initiation/maintenance if the only effect in consideration is the dynamic forcing represented by the mesoscale convergence (assuming that other requisites for convection initiation are fulfilled and the mesoscale forcing is strong enough for the lifting to reach the level of free convection)? Also, how is this diurnal variation conditioned by the presence of the synoptic-scale forcing?
5) Are there subregions that dominate the diurnal cycle of the total dynamic forcing (synoptic plus mesoscale) in terms of total divergence averaged over the entire domain and the whole period studied? And, how do these results compare with those of NGS elaborated using different datasets and methodology?

The focus of this study as in NGS is the diurnal cycle of low-level wind and divergence field (under two different synoptic situations observed during the SALLJEX) within the South American domain encompassed between 20° and 35°S east of the Andes, with emphasis on topographic heights lower than 500 m MSL. Unlike NGS, this paper also focuses on the mesoscale components of circulation, divergences anomalies, spatial variation, and differences in the amplitudes of their diurnal cycle between both synoptic situations studied.

The objective of this paper is to answer the questions posed before to progress in the characterization of the spatial distribution of low-level circulation within the study region beyond the results already obtained by NGS. Because the observational network is coarse and intensive observation campaigns are scarce in the

region, the CFSR provides a good alternative for the study of that atmospheric circulation over an extensive period. Other datasets, with better spatial and temporal resolution than the CFSR, such as reanalysis data from the National Center for Atmospheric Research Climate Four Dimensional Data Assimilation demonstrated ability in representing the diurnal evolution of the mean structure of winds within the planetary boundary layer (PBL) in northern Argentina (Rife et al. 2010). As the present study uses the CFSR, the capability of these reanalyses to represent the diurnal cycles of circulation and divergence in SESA is discussed. This is of interest given their utility in future studies to perform numerical simulations with higher spatial resolution and analyze the atmospheric processes related to the initiation and control of deep moist convection in the region.

This paper is organized as follows: the data, methodology, and regional geography are presented in section 2. A description of the varying synoptic situation using CFSR data is presented in section 3. In section 4, we analyze the results related to the diurnal cycle of low-level winds and associated divergence fields in the subregions of the domain, highlighting the subregions where anomalies dominate low-level circulation. Section 5 discusses the results of this work compared with those of NGS in terms of total divergence and also the possible relationship of the time of occurrence of MCS initiation/maintenance with the timing of maximum low-level convergence within the domain and particularly in the foothills of the Andes and Sierras de Córdoba. Section 6 summarizes our main findings and presents a schematic of the results.

2. Data and methods

The data used in this study are the National Centers for Environmental Prediction CFSR reanalyses, which are available at 64 pressure levels and have a spatial resolution of 0.5° × 0.5° latitude–longitude, with 6-hourly analyses [0600, 1200, 1800, and 0000 UTC, corresponding to 0200, 0800, 1400, and 2000 mountain standard time (MST) at 60°W]. Further information on the CFSR reanalyses can be found in Saha et al. (2010).

The study period starts at 0000 UTC 24 January 2003 and ends at 0000 UTC 8 February 2003, coincident with the period studied by NGS. It covers two weeks with distinct synoptic patterns in each one. These 15 days were selected because they belong to the period covered by the SALLJEX field experiment, which provided major observational data over the SESA region.

To study the diurnal cycle of the mesoscale circulation and its divergence, the horizontal wind is separated in a synoptic component (approximated by the daily mean) and a mesoscale component (approximated by the anomaly with respect to the daily mean). Wind component anomalies and the divergence of the vector anomaly were calculated at each grid point of the domain presented in Fig. 1 for 0000, 0600, 1200, and 1800 UTC. The goal is to identify the influence of the ridges of the Andes and of the lower mountains located east on the diurnal evolution of low-level atmospheric circulation. To this end, and considering a dominant north–south direction of orography in the study domain, the zonal and meridional components of divergence were identified. In particular, averages were calculated of anomalies and divergence in the 50-hPa layer close to the surface (from 950 to 900 hPa in gentle slope areas and from 975 to 925 hPa over the plain). These layers are considered representative of low atmospheric levels.

The domain under study is located in southeastern South America and encompasses gently sloped areas, with altitudes in the range of 100–500 m, and the plain with altitudes below 100 m (Fig. 1). Subregions 1 (Andes) and 2 (Córdoba) are located at the foothills (gentle slopes) of the Andes, which extends from 11°N to 56°S, over the territories of Argentina, Chile, Bolivia, Peru, Ecuador, Colombia, and part of Venezuela in South America, with many peaks of 6000 m MSL and even higher. Subregion 1 has a gentle slope, and encompasses part of Bolivia, Paraguay, and parts of some Argentine provinces. Subregion 2 encloses the Sierras de Córdoba (Argentina). These middle-height mountains extend latitudinally over about 490 km with peaks of up to 2884 m MSL. This subregion is characterized also by the presence of a gap between the Andes and Sierras de Córdoba from 29°S and closed at its southern end at 32°S. The plain region with altitudes below 100 m was divided into northern plain (subregion 3) and southern plain (subregion 4), and were chosen to examine the peculiarities of the diurnal cycle of wind, given that the northern plain is located between both sloped areas and the southern plain is limited by the Sierras de Córdoba in the west and by isolated elevations not exceeding 500 m in the east in Uruguay and southernmost Brazil.

Subregion 5 (Brazilian mountains) spans over part of the territories of Paraguay, Brazil, and Argentina and extends up to the foothills of Serra Geral in Brazil. The western slope of this mountain is gentler than the slopes of subregions 1 and 2. Serra Geral stretches latitudinally and runs along the coast of the Atlantic Ocean, over part of Brazil. The average altitude is 950 m with peaks reaching 1800 m. South of Serra Geral there is an elevated plain that extends over part of Brazil and Uruguay and is called littoral (subregion 6). The southern limit of the domain is 35°S, given that farther south frontal systems are more frequent during the warm season, which restricts the

analysis of the diurnal cycles of wind and divergence to the maritime tropical air mass associated with the western side of the semipermanent anticyclone of the South Atlantic, modified by its incursion into the continent.

3. Synoptic situation

This section briefly describes the synoptic situation during the study period, to provide a characterization of the dominating situations during the diurnal cycles that are analyzed in the following sections. A more detailed synoptic description for this two-week period can be found in Borque et al. (2010) and NGS. The analysis made in the latter paper allowed identifying two different weather situations represented by the composite in Fig. 2. Before 23 January 2003, a frontal system propagated over Argentina. Afterward, high pressure dominated over the entire SESA region, with predominance of dry and stable air. A weak flow from the north and northeast over Argentina associated with the anticyclonic circulation centered over the Atlantic Ocean was not able to advect moist air from lower latitudes because of the cyclone located at about 24°S, confining moister air to low latitudes over Brazil (Fig. 2a). Another characteristic in this week was the convergent northwest–southeast flow over Brazil at 850 hPa (Fig. 2b), associated with the South Atlantic convergence zone (SACZ; Liebmann et al. 2004; Carvalho et al. 2004, and references therein). That SACZ event was considered an intense one given that the cloudiness pattern persisted 15 days, until 30 January, pouring large amounts of rain over southeastern Brazil (e.g., Chaves and Satyamurty 2006). SACZ events associated with strong convection are related to rainfall deficits in subtropical South America (Nogués-Paegle and Mo 1997).

At midlevels (500 hPa), central and northern Argentina was under the influence of a ridge that did not favor convection development (Fig. 2c) and contributed to surface warming. As documented in Cerne et al. (2007), during that week a heat wave—called ''the SALLJEX heat wave'' by those authors—took place, with the highest temperatures recorded over the past 35 years at some Argentine stations. There were no records of convection over SESA until 27 January. By the end of the afternoon of that day, convection was triggered over the Andes, and vanished some hours later (NGS). On 28 January, the passage of a weak frontal system with almost zonal direction south of 33°S triggered convection over the center of Argentina, which vanished during 29 January and did not reach lower latitudes (not shown).

The second period, beginning on 1 February 2003, was characterized by the deepening of the NAL together with the intensification of the SALLJ. Such weather pattern is quite effective in transporting air masses between the tropics and the extratropics, modulating the transport of heat and moisture in SESA (Seluchi and Marengo 2000; Saulo et al. 2004). The NAL, centered at about 27°S east of the Andes (Fig. 2d), expanded its cyclonic flow meridionally, thus favoring warm and moist advection toward the latitudes of the study region. This caused the air mass to destabilize, at least at low levels, and increased convective available potential energy (CAPE) to values higher than the previous week over northern Argentina and southern Brazil (Fig. 2d). A marked SALLJ-related flow from the north and the northeast at 850 hPa brought moisture into central Argentina, where specific humidity increased relative to the values observed in the previous period (Figs. 2b,e). According to NGS, the distinctive feature of this low-level jet event was that both the SALLJ and the NAL core reached higher latitudes than normally in summer (Saulo et al. 2000; Ferreira et al. 2010). At midlevels (500 hPa), large-scale circulation was characterized by zonal flow, with the strongest winds south of 30°S blowing from the west, as shown by the significant geopotential gradient, and with no major areas of vorticity advection (Fig. 2f).

The more unstable conditions and the greater content of moisture observed in the second week caused convective systems to develop over mountains and plains in Argentina starting on 2 February (NGS). During 6 and 7 February, a set of major MCSs developed over central and northern Argentina. Those systems evolved within a scenario that was characterized by the presence of the SALLJ and the proximity of a frontal system south of 32°S (Borque et al. 2010).

Nicolini et al. (2004, 2005, 2006) stratified the SALLJEX data together with the Global Data Assimilation System analysis for the same period in subsamples characterized by different synoptic patterns dominated by the presence of low-level jets bounded by the Andes. The first two samples, Chaco jet event and no-Chaco jet event (CJE and NCJE, respectively), integrate the SALLJ sample and are dominated by the presence of the SALLJ immersed in a low-level poleward flow that extends from equatorial South America latitudes toward subtropical Argentina. The main difference at low levels between them resides in the poleward extension and strength of the jet core (more prominent in CJEs). The third sample, low-level Argentina event (LLJAE), is characterized by a narrow and more localized low-level jet that generates locally over northwestern Argentina. It is immersed in a northerly flow in the west sector of a postfrontal anticyclone located to the east of the Andes. During the two synoptic situations composed for the two different periods of the present

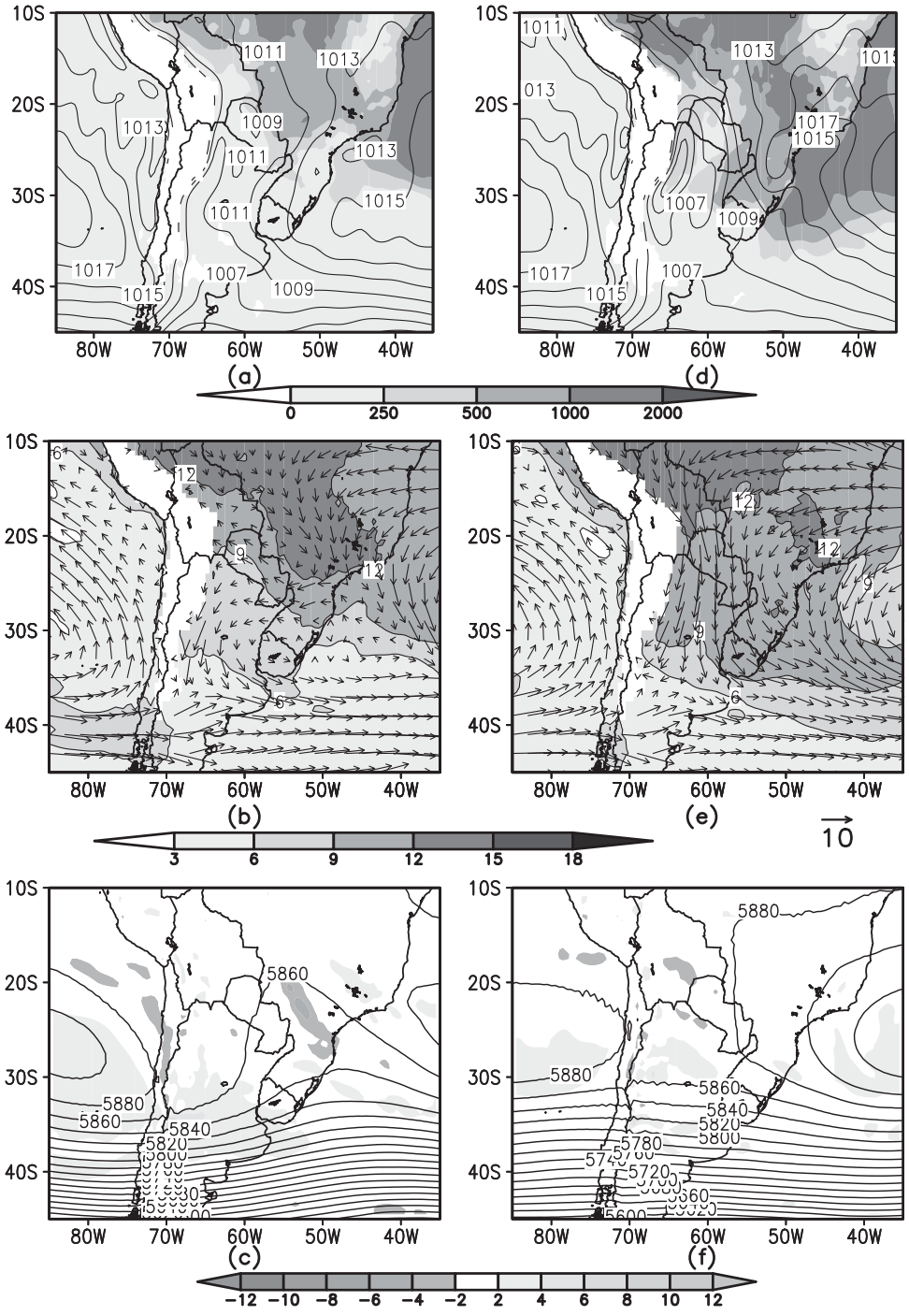

FIG. 2. Composite fields for the periods (left) 24–31 Jan 2003 and (right) 1–7 Feb 2003. (a),(d) Sea level pressure (hPa, contours) and CAPE (J kg^{-1}, shading); (b),(e) wind vectors (m s^{-1}) and specific humidity (g kg^{-1}, shading) at 850 hPa; and (c),(f) geopotential (gpm, contours) and relative vorticity (10^{-5} s^{-1}, shading) at 500 hPa. Values are defined on the scales at the bottom of each panel.

work LLJA events prevailed during the first period, whereas CJEs persisted during the whole second period.

In terms of low-level circulation, the difference between the two synoptic situations is observed in Table 1. During the February week, the northerly subregions (1, 3, and 5) are dominated by a wind with a strong northerly component (signal of the CJE in the synoptic component), whereas in the January week easterlies prevail.

TABLE 1. Average values of synoptic wind speed: zonal (u) and meridional (v) components, and total wind speed (V) at 950 hPa ($m\,s^{-1}$), for each subregion for the periods 24–31 Jan 2003 (Jan) and 1–7 Feb 2003 (Feb).

	Subregion 1		Subregion 2		Subregion 3		Subregion 4		Subregion 5		Subregion 6	
	Jan	Feb	Jan	Feb	Jan	Feb	Jan	Feb	Jan	Feb	Jan	Feb
u	−2.15	−2.25	−2.38	−3.15	−3.95	−1.46	+0.76	−0.69	−2.09	−0.76	−0.24	+1.92
v	−0.26	−7.56	−5.76	−2.53	+0.76	−8.80	−3.78	−4.11	−0.06	−4.46	−1.46	−3.36
V	+2.16	+7.89	+6.23	+4.04	+4.02	+8.92	+3.85	+4.17	+2.09	+4.52	+1.48	+3.87

4. Results

a. Diurnal cycle of low-level wind

Subdaily wind fluctuations in the period under study are shown in Fig. 3, which displays the series of averages over three selected areas of zonal and meridional wind anomalies (mesoscale wind components) with respect to their daily mean. Apparent is the existence of a diurnal cycle in the mesoscale flow as well as a difference in phase between both wind components. This diurnal cycle of wind, as mentioned in the introduction, is coherent with the inertial oscillation mechanism described by Blackadar (1957) and present in the SALLJEX data analysis, by which wind is supergeostrophic at night and subgeostrophic at the times of maximum heating (Nicolini et al. 2004).

The amplitude of the diurnal cycle of these two components changes with changing synoptic patterns (see values in Figs. 3a–c), characterized by a stronger signal during the February week over the whole domain. However, this behavior is more evident near the western mountains (Fig. 3a) and even more critical over the plains (Fig. 3b). During the February week, in the plains (subregions 3 and 4), the difference found in the amplitude with respect to the January week was the largest ($\mathrm{dif}\Delta V' = 3.24\,m\,s^{-1}$, where $\Delta V'$ is the amplitude of the magnitude of the mesoscale wind vector oscillation) and this coincides with the week in which the mean daily winds (synoptic winds) over the plains subregions are stronger (Table 1). This increase in the amplitude of the diurnal oscillation can be explained by the difference in the vertical structure of the PBL in the February week with respect to the previous week. Nicolini et al. (2005, 2006) described the difference in the thermodynamic structure between CJE and LLJAE. Low levels are wetter and convective instability is more clearly defined during CJEs with equivalent potential temperatures in the lower troposphere greater than 10 K with respect to LLJAE environments, which are more vertically restricted because of subsidence associated with dominant anticyclonic conditions. The more efficient turbulent mixing related to a stronger daytime warming in a deeper boundary layer during a CJE effects a daytime stronger frictional retardation of the geostrophic wind. The persistent CJE environment during the second week of the study period (1–7 February 2003) may explain the stronger diurnal oscillation found during this week as the amplitude of the inertial oscillation according to Blackadar (1957) depends on how much subgeostrophic the wind is during the late afternoon and before the wind initiates its nocturnal amplification.

Figure 4 displays the field of wind vector anomaly and the zonal and meridional components at each time of the analysis (0600, 1200, 1800, and 0000 UTC), averaged over the study period. The time progress of the vector wind anomaly in the black box (included in Figs. 4c,f,i,l) resembled a counterclockwise gyre, coherent with the inertial oscillation in the Southern Hemisphere, also observed over practically the entire domain. It is important to clarify that the anomalies shown in Fig. 4 resulted from the average of all the study period, so the direction of the anomalies may be slightly different if we analyze the synoptic situations separately.

In general, the inertial oscillation mechanism produces anomalies from the east and the southeast at 0000 UTC, which progressively turn to northerlies and northeasterlies at 0600 UTC, to westerlies and northwesterlies at 1200 UTC, and to southwesterlies and southerlies at 1800 UTC. In areas that are near the mountains or the oceans, where local thermal effects take place, associated with horizontally inhomogeneous surface, anomalies have a different behavior. This can be seen in Fig. 4, where at 0600 and 1800 UTC the zonal component of the anomalies that are close to the Andes and the Sierras de Córdoba is opposite in direction to that of the anomalies in the valley. In the areas located close to the orography (subregions 1 and 2), anomalies are dominated by nocturnal downslope (katabatic) and daytime upslope (anabatic) winds (Wolyn and McKee 1994 and references therein), which are part of a mountain–plain wind system (Whiteman 2000; American Meteorological Society 2014); while in lower areas (plains, subregions 3 and 4), anomalies are dominated by the effect of inertial oscillation. When these two effects are not in phase, they give rise to a diurnal cycle of wind divergence and convergence.

Close to the ocean, zonal wind anomalies at 0600 and 1800 UTC are opposed to the anomalies in areas located

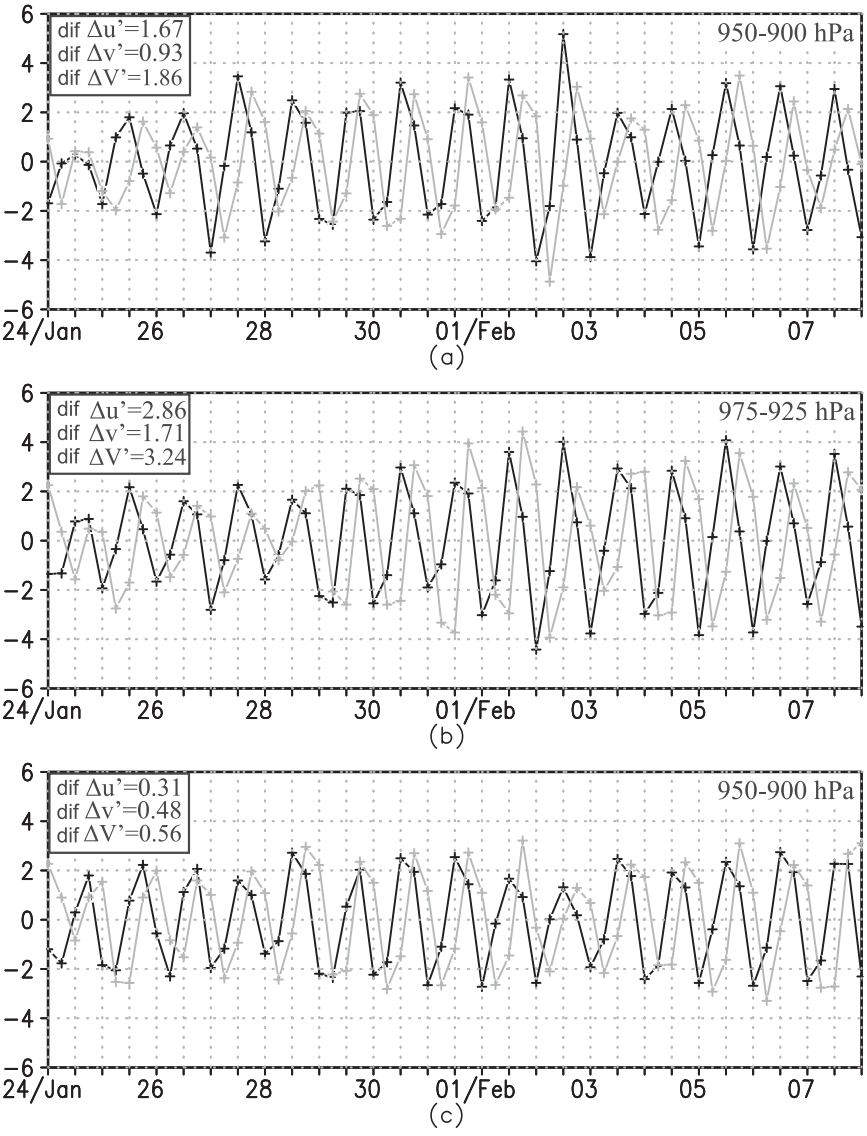

FIG. 3. Time series of average zonal (black) and meridional (gray) mesoscale wind components (m s^{-1}) over (a) subregions 1 and 2 (Andes and Sierras de Córdoba), (b) subregions 3 and 4 (northern and southern plains), and (c) subregions 5 and 6 (Brazilian mountains and littoral). In the inset in the upper-left corner of each panel, the differences in amplitude of the wind oscillations between weeks in February and January (ΔFeb − ΔJan) are indicated for the zonal component (Δu′), meridional component (Δv′), and the magnitude of the mesoscale wind vector (ΔV).

farther inland because of the effect of sea breeze (Figs. 4a,g). The opposite anomalies are also observable in the meridional component in some coastal areas, but with a 6-h lag with respect to the zonal component (Figs. 4e,k). As the regions producing local circulation have a preferred meridional orientation, the zonal component dominates the mesoscale flow. Again, this phase difference in the direction of the anomalies that respond to thermal forcing due to land–sea contrast and inertial oscillation respectively, generate a divergence–convergence cycle.

b. Diurnal cycle of the divergence field

1) ANDES AND SIERRAS DE CÓRDOBA (SUBREGIONS 1 AND 2)

In the subregions located east of the Andes and of the Sierras de Córdoba, at 0600 UTC when inertial oscillation in all the domain produces an anomaly directed toward the west, the katabatic thermal wind over the steep mountain slopes is opposite to this anomaly around 64°W (Fig. 5a) and 62°W (Fig. 5e). The confluence of

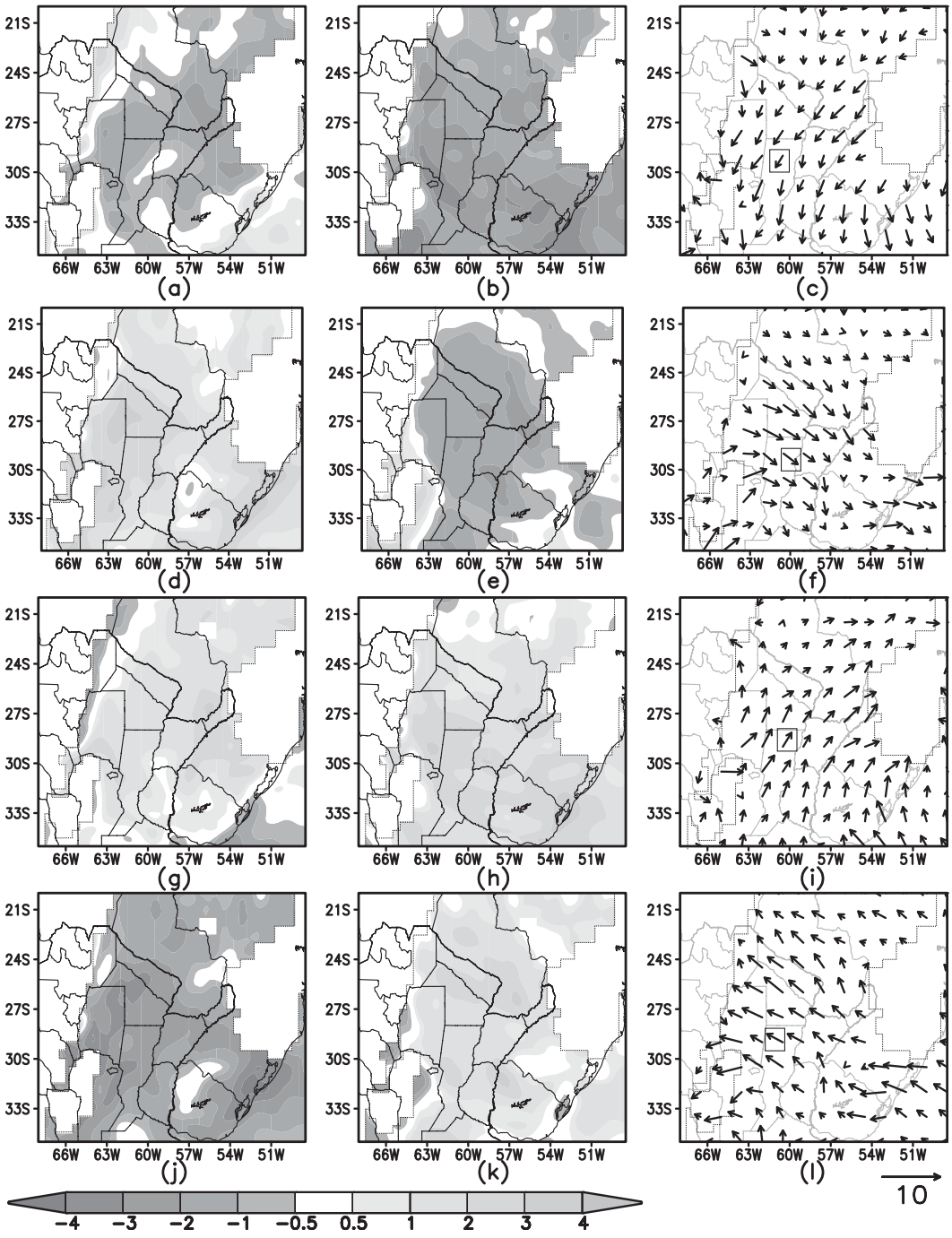

FIG. 4. Hourly average of mesoscale wind components (shaded in meters per second, as defined in the scale at the bottom) at the 950-hPa level from 24 Jan 2003 to 7 Feb 2003 for (top) 0600 UTC (0200 MST), (top middle) 1200 UTC (0800 MST), (bottom middle) 1800 UTC (1400 MST), and (bottom) 0000 UTC (2000 MST): (a),(d),(g),(j) zonal and (b),(e),(h),(k) meridional components and (c),(f),(i),(j) the mesoscale wind vectors (the black boxes highlight the time progress of the wind anomaly at that location). Areas above 500 m are masked (as outlined by dotted borders).

these anomalies produces a large region of mesoscale convergence over the gentle slopes in the subregions 1 and 2. Convergence is favored by the mechanical effect that depends on mountain height, total wind velocity, or static stability that may eventually promote a blocking effect in the total flow. Using CFSR data to determine upstream blocking conditions, the dimensionless Froude number was calculated as $\mathrm{Fr} = U/(NH)$, where U is the

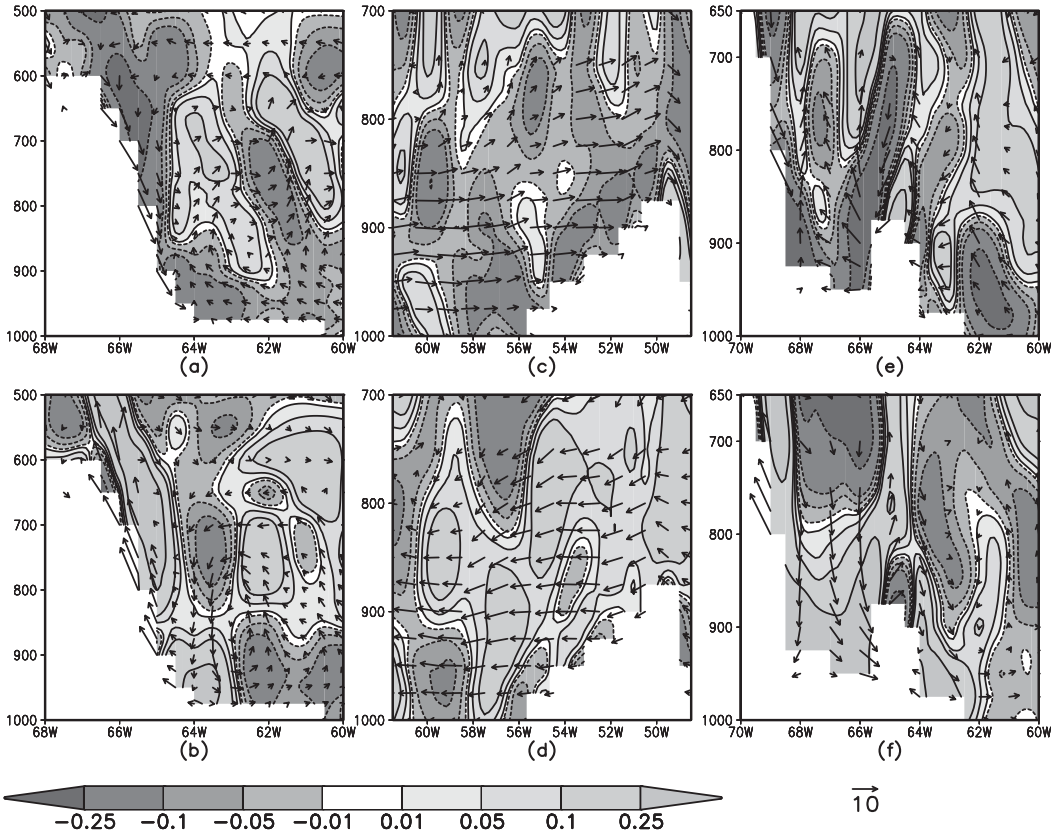

FIG. 5. Vertical cross sections of mesoscale divergence ($\times 10^{-4}\,s^{-1}$ as defined at the scale at the bottom) and mesoscale zonal wind vectors ($m\,s^{-1}$) from 1 to 7 Feb 2003 at latitudes 26.5°S at (a) 0600 UTC (0200 MST) and (b) 1800 UTC (1400 MST); 28°S at (c) 1200 UTC (0800 MST) and (d) 0000 UTC (2000 MST); and 32°S at (e) 0600 UTC (0200 MST) and (f) 1800 UTC (1400 MST).

upstream wind component perpendicular to the mountain, H is the height that the approaching flow needs to achieve to pass over the mountain range, N is the dry Brunt–Väisälä frequency $\{N \equiv [(g/\theta)(\partial\theta/\partial Z)]^{1/2}$, where g is gravitational acceleration, θ is the average absolute potential temperature, and $\partial\theta/\partial z$ is the vertical gradient of potential temperature$\}$. The U and θ values were obtained in the same H layer close to mountains in the upstream flow. The values obtained for 0600 UTC in the low level (950 hPa) of the Andes region are below 0.1, which indicates that the flow turns out to be blocked (Fr $\ll$ 1). Although Fr values are greater in the Córdoba region, the stability conditions present at this time also block upstream flow.

In the valley located between the Andes and the lower mountains in the east (Sierras de Córdoba), there is an area of more intense mesoscale convergence (Fig. 5e). Northerly winds accelerate through this gap between the mountains around 66°W. In addition, winds are forced to ascend but the katabatic wind at this time (mainly zonal winds) from both slopes inhibits ascent. Both the meridional gap wind component and the mountain thermal breeze contribute to the mesoscale convergence shown in Fig. 5e.

Mesoscale convergence in these two subregions controls the net divergence field, where the synoptic component strengthens or weakens the mesoscale divergence field. In subregion 1, east of the Andes, mesoscale convergence in both periods is reinforced by the synoptic convergence (Table 2), given that surface low pressure persists during the two weeks. In subregion 2, the strengthening of the synoptic convergence only takes place during the second week (Table 2).

At 1200 UTC, the wind anomalies that are associated with the inertial oscillation acquire westerly component at the foothills of the Andes within the subregion 1 (Fig. 4f). At this time, the zonal component of the anomalies in the plains (subregion 3) and in the foothills of the Andes (subregion 1) have the same direction (Fig. 4d), causing total wind to acquire a weaker zonal component toward the mountain than at 0600 UTC (Figs. 6a,b, 7a,b), ceasing mesoscale convergence (tables in Figs. 6b, 7b). Given that 1200 UTC is a transition time in the diurnal cycle of anomalies, synoptic

TABLE 2. As in Table 1, but for divergence ($\times 10^{-4}$ s^{-1}).

	Subregion 1		Subregion 2		Subregion 3		Subregion 4		Subregion 5		Subregion 6	
	Jan	Feb	Jan	Feb	Jan	Feb	Jan	Feb	Jan	Feb	Jan	Feb
u	−0.069	−0.017	+0.036	−0.032	+0.011	+0.063	0.010	+0.078	+0.004	−0.004	−0.008	+0.035
v	+0.060	−0.008	+0.001	−0.057	+0.051	−0.041	0.042	−0.110	−0.035	+0.015	+0.058	−0.084
V	−0.008	−0.025	+0.038	−0.089	+0.062	+0.022	0.052	−0.032	−0.031	+0.011	+0.049	−0.048

convergence is more intense in some areas of subregion 1, exceeding the magnitude of mesoscale divergence. In subregion 2, the cycle is also in a transition phase, but mesoscale convergence persists in both periods (tables in Figs. 6b, 7b). However, with the weakening of the anomalies, the contribution of the synoptic component to the net convergence field is greater than at 0600 UTC (Figs. 6a,b, 7a,b).

At the warmest time of the four analyses (1800 UTC), the phase is opposite to that observed at 0600 UTC. Thermally induced circulation now has upslope direction (anabatic) in the Andes and in the Córdoba subregion, and inertial oscillation produces opposite anomalies at low levels over the foothills of the mountains (Figs. 5b,f). This situation gives rise to large divergence areas in the vicinity of the mountains (Figs. 6c, 7c), which characterizes the other phase of the diurnal cycle of divergence in these two subregions. As described for 0600 UTC, anomalies dominate the net divergence field and the contribution of the synoptic component is less in strengthening or weakening the anomalies.

At the end of the cycle (0000 UTC), major areas of mesoscale convergence preceding those found at 0600 UTC, begin to develop in subregions 1 and 2 (Figs. 6d, 7d). At this time, the mechanical effect is more intense, favored by the phase of inertial oscillation that forces total wind toward a direction more perpendicular to the main orientation of the mountains (north–south), as displayed in Fig. 4. Moreover, the anabatic flow of the local circulation is still present at this time (not shown), which favors the flow to reach higher altitudes in the mountains. In the lower mountains (Sierras de Córdoba), besides the stronger zonal wind component, the daytime boundary layer is less stable relative to the other times of the day. Consequently, the higher Froude number flow (Fr $>$ 1) induces crossing of that lower mountain range. When flow moves to the downslope side and reaches the higher Andes it becomes blocked and upstream the Andes convergence is generated in the valley between the two mountain ranges (gap).

2) PLAINS (SUBREGIONS 3 AND 4)

In the plains—subregions 3 and 4—a signal can be observed in the average series that points to a diurnal cycle with mesoscale convergence at night (0600 and 1200 UTC; tables in Figs. 6a,b, 7a,b) and divergence during the day (1800 and 0000 UTC; tables in Figs. 6c,d, 7c,d) in both periods. However, at some times anomalies are so small that it is difficult to identify areas with mesoscale divergence and convergence with a defined diurnal cycle within the subregions. A prevalence of the synoptic-scale forcing over the mesoscale one in the divergence field becomes apparent in these subregions far from orography or coast lines that recurrently drive differential diurnal thermal forcing. Therefore, these subregions are expected to build a weaker mesoscale response. The divergence field seems to be more conditioned by surface inhomogeneities usually characterized by a smaller scale compared with the mountain and the land–sea contrast scales resolved by the reanalysis. In the first week, where the anticyclonic circulation was present throughout much of the domain, synoptic divergence dominated in both subregions (Table 2), and mesoscale nocturnal convergences are not strong enough to modulate the net divergence (Figs. 6a,b). In the second week in subregion 3 the synoptic divergences are less intense (Table 2) and this facilitates the mesoscale nocturnal convergences to exceed the 1200 UTC synoptic divergences (Fig. 7b). However, in subregion 4 there was a dominance of synoptic convergence in the decelerating exit area of the low-level jet, enhancing the mesoscale nocturnal convergences previously mentioned (Figs. 7a,b). This would indicate the dominant role of the SALLJ in the initiation of convection and the interdependence between the diurnal cycle of the SALLJ and the diurnal cycle of convection initiation–maintenance in subregion 4.

3) BRAZILIAN MOUNTAINS (SUBREGION 5)

In the east of the domain, where the Brazilian mountains (subregion 5) are located, inertial oscillation and thermal circulation over the hills, near the surface, are in the same direction (Figs. 5c,d). This leads to results that differ from those obtained for the vicinity of subregions 1 and 2.

At 0600 UTC, over the western slope of the mountains, local circulation is in its nocturnal phase (katabatic flow) and gives rise to wind anomalies with easterly zonal component (not shown). This direction coincides

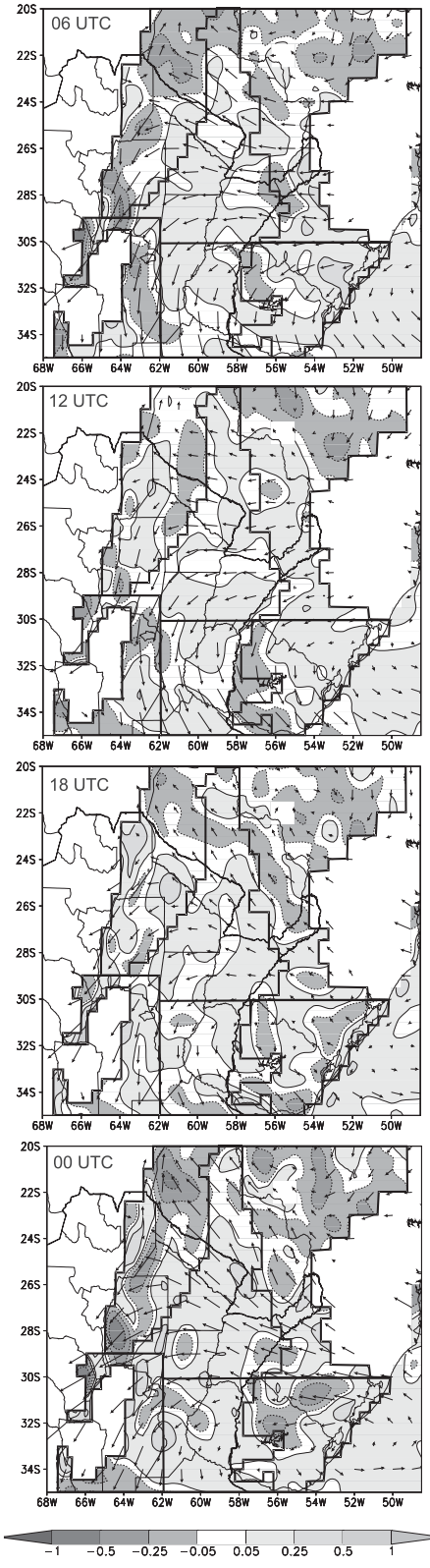

(a)

	subregion 1		subregion 3		subregion 5	
	div′	div	div′	div	div′	div
u	−0.055	−0.123	−0.019	−0.008	+0.006	+0.010
v	+0.009	+0.069	+0.000	+0.051	−0.005	−0.040
V	−0.046	−0.054	−0.019	+0.043	+0.001	−0.030
	subregion 2		subregion 4		subregion 6	
	div′	div	div′	div	div′	div
u	−0.085	−0.049	−0.022	−0.013	+0.021	+0.013
v	−0.020	−0.018	+0.005	+0.048	+0.026	+0.084
V	−0.105	−0.067	−0.017	+0.035	+0.048	+0.097

(b)

	subregion 1		subregion 3		subregion 5	
	div′	div	div′	div	div′	div
u	+0.003	−0.066	−0.013	−0.002	−0.002	+0.002
v	+0.017	+0.077	−0.003	+0.049	+0.002	−0.034
V	+0.020	+0.011	−0.016	+0.046	−0.001	−0.032
	subregion 2		subregion 4		subregion 6	
	div′	div	div′	div	div′	div
u	−0.031	+0.005	−0.017	−0.007	+0.007	−0.001
v	−0.026	−0.024	−0.015	+0.027	−0.002	+0.055
V	−0.057	−0.019	−0.032	+0.020	+0.005	+0.054

(c)

	subregion 1		subregion 3		subregion 5	
	div′	div	div′	div	div′	div
u	+0.080	+0.012	+0.009	+0.020	−0.008	−0.004
v	−0.021	+0.039	−0.009	+0.042	+0.007	−0.029
V	+0.059	+0.051	+0.000	+0.062	−0.001	−0.032
	subregion 2		subregion 4		subregion 6	
	div′	div	div′	div	div′	div
u	+0.081	+0.117	+0.012	+0.022	−0.017	−0.025
v	+0.033	+0.034	−0.005	+0.038	−0.011	+0.046
V	+0.113	+0.151	+0.008	+0.060	−0.028	+0.021

(d)

	subregion 1		subregion 3		subregion 5	
	div′	div	div′	div	div′	div
u	−0.028	−0.097	+0.023	+0.034	+0.004	+0.008
v	−0.005	+0.056	+0.011	+0.062	−0.004	−0.039
V	−0.033	−0.041	+0.034	+0.096	+0.001	−0.031
	subregion 2		subregion 4		subregion 6	
	div′	div	div′	div	div′	div
u	+0.035	+0.071	+0.027	+0.037	−0.012	−0.020
v	+0.013	+0.015	+0.014	+0.057	−0.013	+0.045
V	+0.048	+0.086	+0.041	+0.093	−0.024	+0.025

FIG. 6. Hourly average total divergence ($\times 10^{-4}$ s^{-1}, shaded as defined at the scale at the bottom) and total wind vectors (m s^{-1}) at the 950-hPa level for (a) 0600 (0200 MST), (b) 1200 (0800 MST), (c) 1800 (1400 MST), and (d) 0000 UTC (2000 MST) between 24 and 31 Jan 2003. Regions above 500 m are masked in white and correspond to the Andes Mountains, Córdoba, and Serra Geral in Fig. 1. The average values of the zonal (u), meridional (v), and total (V) components of the mesoscale (div′) and total (div) divergence for each subregion 1–6 are shown in the tables to the right of the panels.

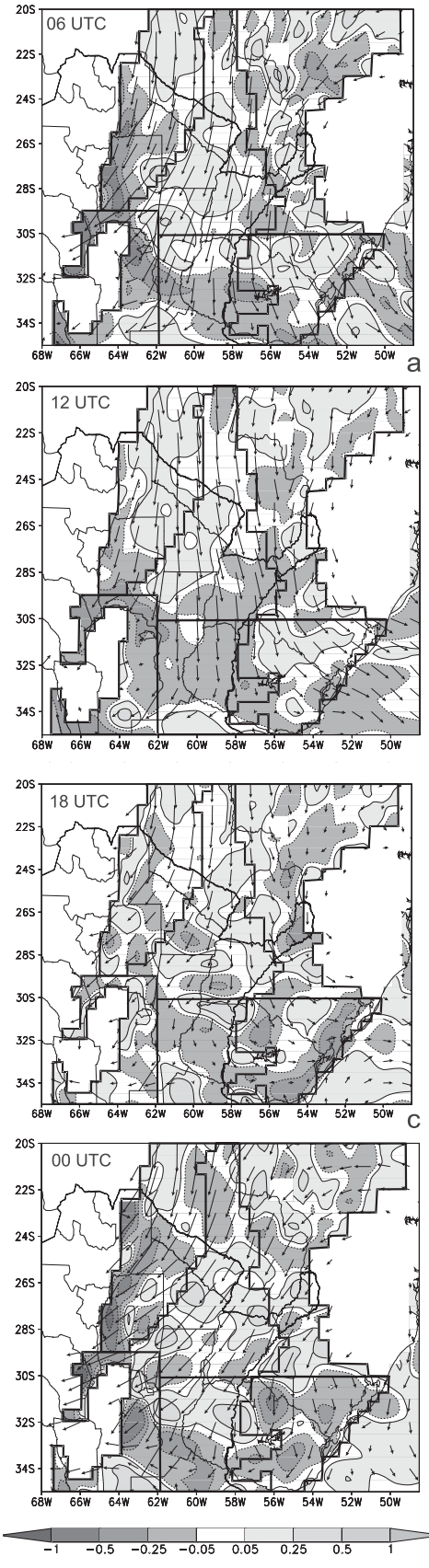

(a)

	subregion 1		subregion 3		subregion 5	
	div'	div	div'	div	div'	div
u	-0.040	-0.057	-0.012	+0.050	-0.008	-0.012
v	+0.024	+0.015	+0.009	-0.032	+0.005	+0.020
V	-0.016	-0.041	-0.004	+0.018	-0.003	+0.008

	subregion 2		subregion 4		subregion 6	
	div'	div	div'	div	div'	div
u	-0.090	-0.121	+0.041	+0.119	+0.027	+0.062
v	-0.047	-0.104	-0.057	-0.167	+0.015	-0.069
V	-0.137	-0.225	-0.015	-0.048	+0.042	-0.007

(b)

	subregion 1		subregion 3		subregion 5	
	div'	div	div'	div	div'	div
u	+0.039	+0.022	-0.020	+0.043	-0.018	-0.022
v	+0.008	+0.000	-0.008	-0.048	-0.001	+0.015
V	+0.048	+0.022	-0.027	-0.006	-0.018	-0.007

	subregion 2		subregion 4		subregion 6	
	div'	div	div'	div	div'	div
u	-0.038	-0.070	-0.028	+0.049	+0.053	+0.088
v	+0.003	-0.054	-0.012	-0.122	-0.007	-0.091
V	-0.035	-0.124	-0.041	-0.073	+0.045	-0.003

(c)

	subregion 1		subregion 3		subregion 5	
	div'	div	div'	div	div'	div
u	+0.056	+0.039	+0.024	+0.087	+0.006	+0.002
v	-0.017	-0.026	-0.008	-0.049	-0.019	-0.003
V	+0.038	+0.013	+0.016	+0.038	-0.012	-0.001

	subregion 2		subregion 4		subregion 6	
	div'	div	div'	div	div'	div
u	+0.114	+0.082	-0.016	+0.062	-0.038	-0.003
v	+0.071	+0.014	+0.060	-0.050	-0.021	-0.104
V	+0.185	+0.096	+0.043	+0.011	-0.059	-0.107

(d)

	subregion 1		subregion 3		subregion 5	
	div'	div	div'	div	div'	div
u	-0.055	-0.072	+0.008	+0.071	+0.019	+0.015
v	-0.015	-0.023	+0.007	-0.034	+0.015	+0.030
V	-0.070	-0.096	+0.015	+0.037	+0.034	+0.045

	subregion 2		subregion 4		subregion 6	
	div'	div	div'	div	div'	div
u	+0.014	-0.018	+0.003	+0.081	-0.042	-0.006
v	-0.026	-0.083	+0.010	-0.101	+0.013	-0.070
V	-0.012	-0.101	+0.013	-0.019	-0.028	-0.077

FIG. 7. As in Fig. 6, but for the period 1–7 Feb 2003.

with the anomalies induced by the inertial oscillation acting over the plain (subregion 3, Fig. 4c). These mechanisms reinforce mutually favoring mesoscale divergence on the western slopes of the mountains and mesoscale convergence over the plain (subregion 3, tables in Figs. 6a, 7a). The latter is also observable, near the surface, at 0000 UTC (Fig. 5d).

The opposite phase occurs at 1200 and 1800 UTC, when inertial oscillation drives total wind toward the mountains and is strengthened by the thermal component over the slopes (anabatic flow). Given that flow in the January week is easterly (Figs. 6b,c), anomalies tend to stop total wind, and, in the February week, when flow is northerly they divert total wind toward the mountains (Figs. 7b,c). Such situations give rise to mesoscale convergence over the slope as well as over lower areas located close to the plains (Fig. 5c). These anomalies are weaker than in subregions 1 and 2. This makes the total divergence field dependent on the magnitude of the synoptic component, as in subregions 3 and 4 (tables in Figs. 6b,c, 7b,c). In the January week, the mean value in this subregion (Table 2) indicates synoptic convergence prevalence mainly by the low pressure zone influence to the north of 25°S (Fig. 2a), while in the February week the synoptic divergence predominates (Table 2).

4) LITTORAL (SUBREGION 6)

In the littoral area, mesoscale divergence occurs at 0600 and 1200 UTC during both synoptic regimes. At these times, the deflection of wind toward the Atlantic Ocean is coherent with the land breeze. This becomes evident at 0600 UTC around 33°S (Fig. 4a), when the mesoscale eastward zonal component decreases with increasing distance from the ocean, generating positive divergence (tables in Figs. 6a, 7a). With the approaching of the warmest analysis time (1800 UTC), anomalies induced by inertial oscillation have a zonal component that is opposite to breeze anomalies (Fig. 4g), causing mesoscale convergence to dominate the coastal strip (Figs. 6c, 7c). At the end of the cycle (0000 UTC), convergence weakens because of the weakening of the thermal component that the anomaly had toward the continent. This indicates that although mesoscale convergence continues to dominate at this time, the cycle starts its transition to the nocturnal divergence phase (tables in Figs. 6d, 7d).

It is worth clarifying that the diurnal cycle of the mesoscale divergence field in this subregion is mostly dominated by the synoptic component in both periods. However, in the coastal strip, mesoscale convergence at 1800 UTC—associated with the diurnal cycle of sea breeze—is stronger and modulates the total divergence field (Figs. 6c, 7c). For this subregion as well as in the subregion 4, the synoptic component was divergent in the January week and convergent in the February week (Table 2).

5. Discussion

a. *Comparison of the averaged diurnal cycle with the one obtained by NGS*

Taking into account differences in the analysis and methodology and slight differences in the limits of domain used, the results of this work are compared with those of NGS in terms of total divergence averaged over the entire domain and throughout the 15-day period studied. According to CFSR data, divergence dominates at daytime and is mainly contributed by the zonal component (Fig. 8a). This agrees with the results obtained by NGS in spite of the differences in time resolution (Fig. 8b). On the other hand, there is a difference in the results during the nocturnal hours. Both CFSR and BRAMS-20 exhibit convergence but while current work finds a similar contribution of both wind components, NGS results indicate that nocturnal convergence is completely affected by the meridional component and zonal contribution can be ignored. Regional variability becomes evident when the region is divided into subregions, where cycles are not in phase (not shown). As discussed in section 4, subregions have their own cycles, given that they are affected by different mechanisms. The plain subregions (subregions 3 and 4) present a convergence maximum 6 h after the subregions 1 and 2, and the lag is of 12 h when comparing these subregions with subregion 6. The divergence diurnal cycle shown in Fig. 8a is strongly conditioned by the divergence diurnal cycle of subregion 2. This divergence cycle in subregion 2 presents a magnitude of higher order than in the other subregions, mainly in the February week (see tables in Figs. 7a–d and Table 3).

b. *Relationship between low-level dynamical forcing and precipitation/convection*

After the analysis related to the diurnal cycle of low-level wind and divergence described in section 4 we return to the question raised in the introduction, namely, which diurnal cycle of deep moist convection would be expected in the different subregions in terms of initiation/maintenance. Mesoscale convergence is the only forcing that this question takes in consideration. Besides, it is hypothesized that other requisites for convection initiation are fulfilled and the mesoscale forcing is strong enough for the lifting to reach the level of free convection. Existing literature on the initiation of deep convection in the study region is scarce and identification

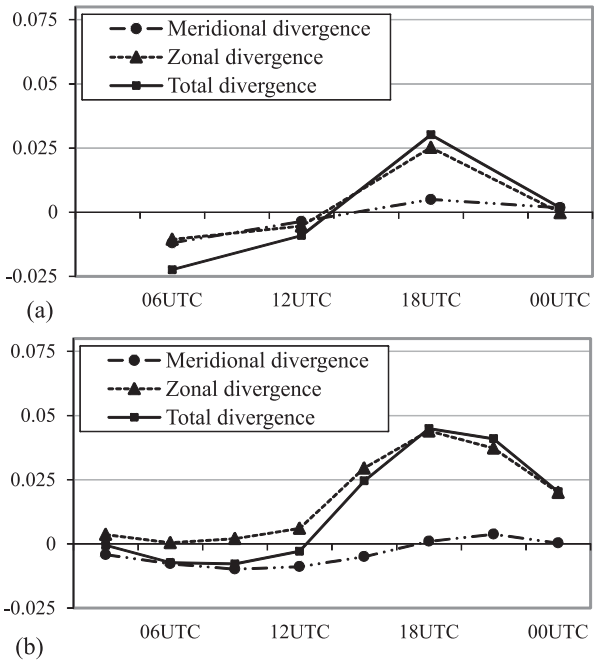

FIG. 8. Total, zonal, and meridional divergence ($\times 10^{-4}\,s^{-1}$) averaged for all regions for the 15-day study period: (a) current study and (b) adapted from NGS.

of convection is based on different assumptions and criteria depending on the availability of radar and/or satellite data.

Focusing on subregions 1 (Andes) and 2 (Sierras de Córdoba), given that these areas provided more evidence about the diurnal cycle in the anomalies that modulates the total divergence field, Vila (2005) determined the paths of 33 MCSs identified by satellite IR brightness temperatures below 235 K and 24-h precipitation above 25 mm. The average location of initiation of these MCSs, which during the mature stage cross over Uruguay, is in the domain of subregion 2. Although the frequency of initiation times was not identified in the sample, the author indicates that this is an MCS genesis area. On the other hand, Salio and Nicolini (2006), on the basis of satellite brightness temperatures below 218 K, found that convection was more frequent east of the Andes and east of the Sierras de Córdoba from nightfall to 0600 UTC in summer. Romatschke and Houze (2010), using the TRMM PR product, analyzed the diurnal cycle of the probability of occurrence of deep convective cores and other types of extreme convective systems in South America. To this end, they selected the southern foothills of the central Andes, apart from six other subregions. The geographic location of this area is similar to that of subregions 1 and 2. They found a higher frequency of deep and wide convective cores (reflectivity values of 40 dBZ or greater) between 1900 and 0300 UTC over the Sierras de Córdoba and in the foothills of the Andes. Although the times at which the maximum probability of occurrence of the deep convective cores found by those authors agree with those of maximum mesoscale convergence in the same areas in this study, Romatschke and Houze (2010) did not determine the most frequent times of initiation of those cores. In other work, L. Vidal (2014, personal communication) uses a methodology that combines orbital data with radar precipitation features (RPFs; Liu et al. 2007) of TRMM and the Forecast and Tracking the Evolution of Cloud Clusters technique (ForTraCC; Vila et al. 2008), which is based on tracking a cloud system defined from satellite imagery in the infrared thermal range. Different levels were defined for RPF extreme events (5%, 1%, 0.1%, and 0.01%) based on seven proxies related to the capacity to produce precipitation and the intensity of associated convection: total volumetric precipitation, minimum temperature at 37 and 85 GHz, and rate of electrical discharges. In addition, Vidal performed a characterization of the life cycle of those convective systems. Identification of cases included in Vidal's sample that were triggered in subregions 1 and 2 of this paper revealed that 77% of these 149 convective systems had started between 1900 and 0600 UTC.

As to the current study, a detailed analysis of the evolution of organized convection using GOES data over the domain during the February week (not included)

TABLE 3. Amplitudes of mesoscale divergences oscillations (Δd) and differences (Dif) ($\times 10^{-4}\,s^{-1}$) between the January and February weeks for the zonal and meridional components and the total divergence.

	January			February			Dif (ΔFeb − ΔJan)		
Subregion	Δdu′	Δdv′	ΔdV′	Δdu′	Δdv′	ΔdV′	Dif(Δdu′)	Dif(Δdv′)	Dif(ΔdV′)
1	0.135	0.038	0.173	0.111	0.041	0.152	−0.024	0.003	−0.021
2	0.165	0.058	0.224	0.203	0.118	0.321	0.038	0.060	0.097
3	0.042	0.020	0.062	0.044	0.017	0.061	0.002	−0.003	−0.001
4	0.049	0.029	0.079	0.070	0.117	0.187	0.020	0.087	0.108
5	0.014	0.012	0.026	0.037	0.033	0.070	0.023	0.022	0.044
6	0.038	0.039	0.077	0.094	0.036	0.130	0.056	−0.003	0.053

found MCSs mostly limited to the southern subregions that developed at the exit region of the SALLJ. Some of those MCSs initiated in the afternoon over the western mountains and moved through subregions 2, 4, and 6 in their progression toward the east while intensifying (especially in the ''gap'') and/or generating new cores. Some developed southward of 35°S and entered subregion 4 during their expansion. TRMM 3B42V7 (Huffman et al. 2007) estimated hourly precipitation fields exhibit maxima at the times when both mesoscale and synoptic convergence contribute to the dynamic forcing and minima when mesoscale divergence dominates over synoptic convergence (Fig. 9). To investigate this coincidence in time between an enhancement or maintenance of precipitation and maximum convergence in each southern subregion, we compared the amplitude of daily cycle in mesoscale convergence in these subregions during the two weeks to explore a possible relationship between the dynamical forcing and the presence of precipitation during the February week. We found an increase in the strength of the daily cycle during the February week that maximizes in these subregions, contributed mostly by the meridional component in subregions 2 and 4 and by the zonal component in subregion 6 (Table 3). A possible mechanism capable of producing this amplification is the feedback between maximum rainfall generated by large MCSs and low-level flow at the exit region of a CJE investigated in this region by Saulo et al. (2004, 2007). According to this mechanism, the predominantly northerly low-level wind accelerates because of the latent heating released in the MCS area, extends more to the south, and promotes stronger low-level convergence that in turn intensifies convection. During the February week, the 850-hPa wind field exhibits two nocturnal low-level maxima when large MCSs occur, a northerly one more related to inertial oscillation and a southerly one where this mechanism superposes to inertial oscillation. As this mechanism maximizes at the time of maximum precipitation, it positively reinforces the mesoscale convergence enhancing the diurnal cycle of mesoscale forcing. As to the components that mostly contribute to the amplification of this cycle, the meridional component is the preferred one in subregions 2 and 4 as the SALLJ axis is meridionally oriented in these areas. The amplification of the zonal component (more related to the sea breeze) in subregion 6 is partially effected by a stronger divergence at night because of the presence of MCSs in subregion 4 and/or is effected by the upstream area of an LLJ core located over the Atlantic during the February week (not shown). At daytime hours convergence is stronger because of the enhancement of MCSs over Uruguay.

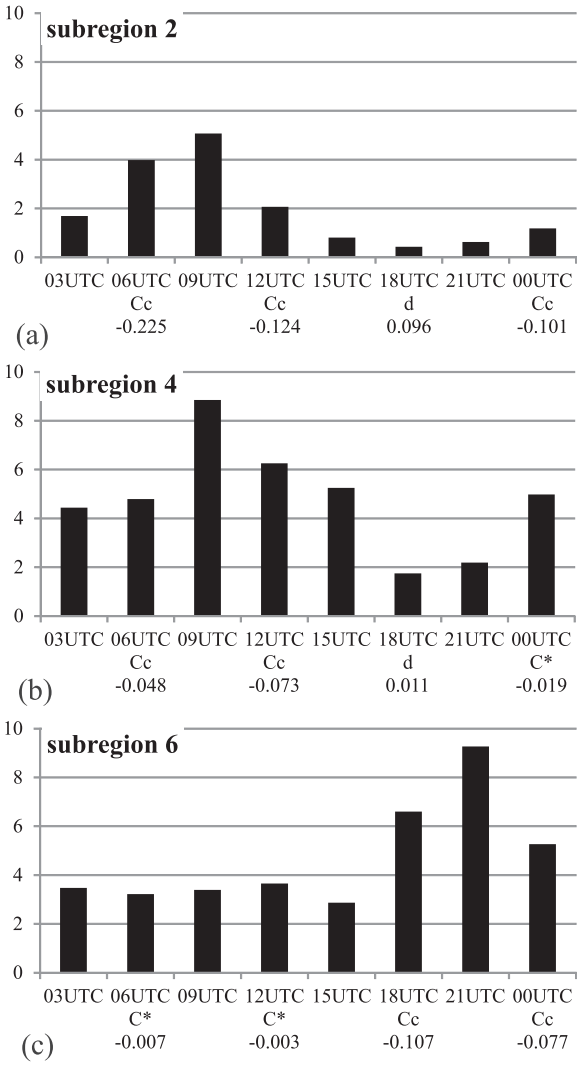

FIG. 9. Diurnal variation (1–7 Feb 2003) of hourly 3B42V7 accumulated rainfall estimation (mm) averaged for subregions (a) 2, (b) 4, and (c) 6. At the bottom of each subpanel, the letters at the principal times are defined as C* = dominant synoptic convergence and + mesoscale divergence, Cc = synoptic and mesoscale convergence, and d = dominant mesoscale divergence + synoptic convergence; the numbers indicate total divergence ($\times 10^{-4}$ s^{-1}).

6. Summary

The scope of this study is to progress in the characterization of the low-level mesoscale components of circulation, their divergences, spatial variation over a subdomain of SESA, and differences in the amplitudes of their diurnal cycle between two synoptic situations during SALLJEX, using CFSR reanalyses. We summarize in this section the answers to the questions posed in the introduction based on the results found in sections 4 and 5. The decomposition of wind analysis in a synoptic

TABLE 4. Summary of the total divergence phase and contribution of the synoptic and mesoscale components according to the values in Figs. 6 and 7 for each subregion for the periods 24–31 Jan 2003 (Jan) and 1–7 Feb 2003 (Feb): D* = dominant synoptic divergence + mesoscale convergence; C* = dominant synoptic convergence + mesoscale divergence; Dd = synoptic and mesoscale divergence; Cc = synoptic and mesoscale convergence; d = dominant mesoscale divergence and synoptic convergence; c = dominant mesoscale convergence and synoptic divergence; D = synoptic divergence; C = synoptic convergence.

	Subregion 1		Subregion 2		Subregion 3		Subregion 4		Subregion 5		Subregion 6	
UTC	Jan	Feb	Jan	Feb	Jan	Feb	Jan	Feb	Jan	Feb	Jan	Feb
0600	Cc	Cc	c	Cc	D*	D*	D*	Cc	C*	D*	Dd	C*
1200	d	d	c	Cc	D*	c	D*	Cc	Cc	c	Dd	C*
1800	d	d	Dd	d	D*	Dd	Dd	d	Cc	c	D*	Cc
0000	Cc	Cc	Dd	Cc	Dd	Dd	Dd	C*	C*	Dd	D*	Cc
Synoptic	C	C	D	C	D	D	D	C	C	D	D	C

and a mesoscale components support the existence of a mesoscale wind diurnal forcing. On the slopes and on the coast, the cycle is forced by breeze systems, and on the plain the diurnal cycle is clearly driven by inertial oscillation. However, this diurnal cycle does not exhibit a substantial amplitude difference among subregions during each synoptic situation. This modest spatial variation is partly explained by the west–east extension of the selected subregions near the westerly mountains and near the coast as both the inertial oscillation (with the same direction as over the plains) and the thermal mesoscale breeze opposes within the same subregion. These opposite directions reduce the amplitude of wind diurnal cycle in those subregions. In contrast with this result, the selection of subregions denotes more clearly the mesoscale divergence spatial variability that manifests in stronger diurnal cycles in subregion 1, 2, 4, and 6.

Differences in the amplitude of diurnal cycle between synoptic situations for the mesoscale wind circulation and for the divergences are addressed. Stronger diurnal response in the circulation during the wetter February week is ascribed to more efficient turbulent mixing in a deeper boundary layer related to stronger daytime warming, whereas larger amplitudes in divergence diurnal cycle in the same week are explained in terms of a feedback mechanism previously studied in the region, between a strong low-level jet core and precipitation related to organized nocturnal convection at the exit of this current. This mechanism enhances both the intensity of low-level convergence and of MCSs precipitation dominantly at night in subregions 2 and 4.

Addressing the relationship between diurnal variation of initiation/maintenance of deep moist convection and total convergence forcing (synoptic plus mesoscale), Table 4 summarizes the results analyzed in previous sections in terms of the phase of this variable in the different subregions. Differences are found between synoptic situations at the same subregion, more evident for those where precipitation occurred during the wetter February week. In subregions 1 and 2 convergence associated with the diurnal cycle is more intense than its synoptic component and modulates the net divergence in the fully diurnal cycle even during the drier January week. In general over the other subregions the mesoscale convergence forcing strengthens or weakens the effect of the synoptic forcing.

We also attempted to identify the diurnal cycle of the divergence field associated with the mesoscale circulation, in order to relate convergence phases with areas of likely genesis and/or maintenance of MCSs. Figure 10 outlines the different components of mesoscale circulation and associated divergence patterns, analyzed in section 4. Outstandingly, the most evident diurnal cycle in the divergence fields is restricted to areas located close to the mountains. When a mesoscale wind component forced by the inertial oscillation mechanism that dominates over the plains is directed toward the mountains, it induces convergence at the foothills of high mountains. In the afternoon, convergence strips parallel to the coast and convergence over the Andes, Sierras de Córdoba, and Serra Geral are also depicted in Fig. 10.

The relationship between regional variability of diurnal cycle of thermal and dynamical forcings and their related convergence zones and convection in the region is also addressed. A review of the literature related to initiation/maintenance of convection more specifically focused in the western subregions is included and a synthesis of a combined analysis of convergence and precipitation occurred during the February week over the southern subregions is presented highlighting the role of the precipitation in enhancing the diurnal cycle of mesoscale convergences.

Analyzing the total divergence diurnal variation averaged over the entire domain and the whole 15-day period, the results are similar to those already found by NGS and are coherent with the prevalence of nocturnal deep organized convection in this region. However,

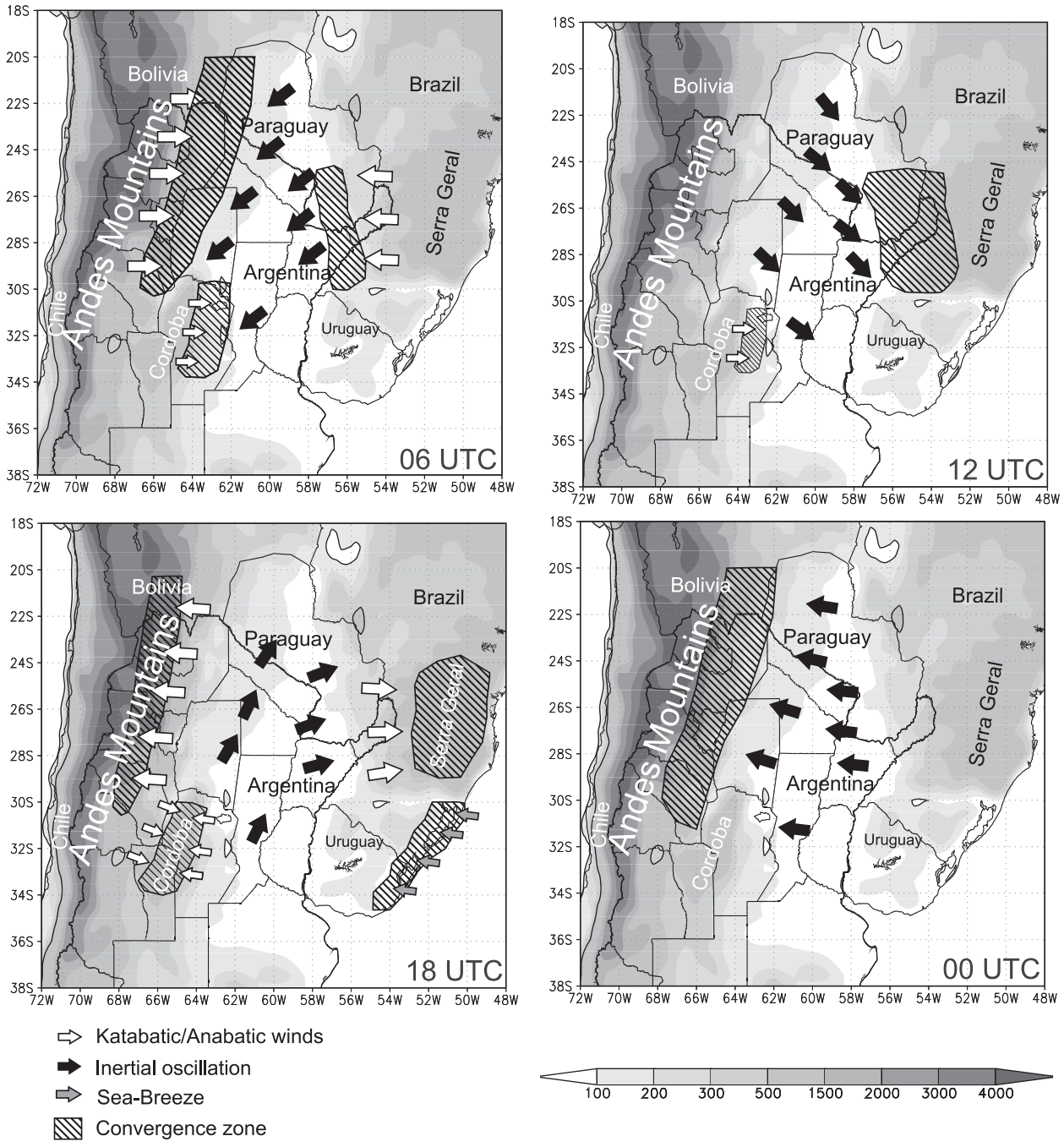

FIG. 10. Schematic of the regional variability of the diurnal cycle of mountain–plain and sea breezes, inertial oscillation, and convergence zones. Topography is shaded, and values are defined by the scale at the bottom.

when this analysis focused on the different subregions we found that they have their own cycles, given that they are affected by different mechanisms, with a stronger signal in subregion 2. These specific cycles may change in low-level jet situations characterized by a SALLJ core located northward of the position found in this study and when MCSs and related precipitation occur more typically over subregion 3 instead than in the southern subregions.

Acknowledgments. The authors acknowledge Dr. Luciano Vidal for supplying his processed dataset with the position and timing of initiation of observed subtropical extreme mesoscale convective systems in South America. This

work was supported by Argentina Grants ANPCyT PICT 2007-00355, Universidad de Buenos Aires UBACyT 2011-2014 W742, and Consejo Nacional de Investigaciones Científicas y Técnicas PIP 2010-2012 11220090100850.

REFERENCES

American Meteorological Society, cited 2014: ''Mountain–plains wind systems.'' Glossary of Meteorology. [Available online at http://glossary.ametsoc.org/wiki/Mountain-plains_wind_systems.]

Arritt, R. W., T. D. Rink, M. Segal, D. P. Todey, C. A. Clark, M. J. Mitchell, and K. M. Labas, 1997: The Great Plains low-level jet during the warm season of 1993. *Mon. Wea. Rev.,* **125,** 2176–2192, doi:10.1175/1520-0493(1997)125<2176:TGPLLJ>2.0.CO;2.

Banta, R. M., 1990: The role of mountain flows in making clouds. *Atmospheric Processes over Complex Terrain, Meteor. Monogr.,* No. 45, 229–283.

Berri, G., and J. Inzunza, 1993: The effect of the low-level jet on the poleward water vapour transport in the central region of South America. *Atmos. Environ.,* **27A,** 335–341, doi:10.1016/0960-1686(93)90107-A.

Blackadar, A. K., 1957: Boundary layer wind maxima and their significance for the growth of nocturnal inversions. *Bull. Amer. Meteor. Soc.,* **38,** 283–290.

Bonner, W. D., and J. Paegle, 1970: Diurnal variations in boundary layer winds over the south-central United States in summer. *Mon. Wea. Rev.,* **98,** 735–744, doi:10.1175/1520-0493(1970)098<0735:DVIBLW>2.3.CO;2.

Borque, P., P. Salio, M. Nicolini, and Y. García Skabar, 2010: Environment associated with deep moist convection under SALLJ conditions: A case study. *Wea. Forecasting,* **25,** 970–984, doi:10.1175/2010WAF2222352.1.

Carvalho, L. M. V., C. Jones, and B. Liebmann, 2004: The South Atlantic convergence zone: Intensity, form, persistence, and relationships with intraseasonal to interannual activity and extreme rainfall. *J. Climate,* **17,** 88–108, doi:10.1175/1520-0442(2004)017<0088:TSACZI>2.0.CO;2.

Cerne, S. B., C. S. Vera, and B. Liebmann, 2007: The nature of a heat wave in eastern Argentina occurring during SALLJEX. *Mon. Wea. Rev.,* **135,** 1165–1174, doi:10.1175/MWR3306.1.

Chaves, R. R., and P. Satyamurty, 2006: Study of the regional conditions associated with a strong SACZ event during January 2003 (in Portuguese). *Rev. Bras. Meteor.,* **19,** 89–98.

Conforte, J. C., 1997: A study of mesoscale convective complexes over South America (in Portuguese). Ph.D. thesis, National Institute for Space Research, Brazil, 112 pp.

Cotton, W. R., and Coauthors, 2003: RAMS 2001: Current status and future directions. *Meteor. Atmos. Phys.,* **82,** 5–29, doi:10.1007/s00703-001-0584-9.

Douglas, M. W., M. Nicolini, and C. A. Saulo, 1998: Observational evidences of a low level jet east of the Andes during January-March 1998. *Meteorologica,* **23,** 63–72.

Ferreira, L., C. A. Saulo, and M. Seluchi, 2010: Features of the northwestern Argentinean low during the 1997-2003 period: Selection criteria and statistical analysis (in Spanish). *Meteorologica,* **35,** 17–28.

Freitas, S. R., and Coauthors, 2009: The Coupled Aerosol and Tracer Transport model to the Brazilian developments on the Regional Atmospheric Modeling System (CATT-BRAMS). Part 1: Model description and evaluation. *Atmos. Chem. Phys.,* **9,** 2843–2861, doi:10.5194/acp-9-2843-2009.

García Skabar, Y., and M. Nicolini, 2009: Enriched analyses with assimilation of SALLJEX data. *J. Appl. Meteor. Climatol.,* **48,** 2425–2440, doi:10.1175/2009JAMC2091.1.

Houze, R. A., 2012: Orographic effects on precipitating clouds. *Rev. Geophys.,* **50,** RG1001, doi:10.1029/2011RG000365.

Huffman, G. J., and Coauthors, 2007: The TRMM multi-satellite precipitation analysis: Quasi-global, multi-year, combined-sensor precipitation estimates at fine scale. *J. Hydrometeor.,* **8,** 38–55, doi:10.1175/JHM560.1.

Kummerow, C., W. Barnes, T. Kozu, J. Shiue, and J. Simpson, 1998: The Tropical Rainfall Measuring Mission (TRMM) sensor package. *J. Atmos. Oceanic Technol.,* **15,** 809–817, doi:10.1175/1520-0426(1998)015<0809:TTRMMT>2.0.CO;2.

Liebmann, B., G. N. Kiladis, C. S. Vera, A. C. Saulo, and L. M. V. Carvalho, 2004: Subseasonal variations of rainfall in South America in the vicinity of the low-level jet east of the Andes and comparison to those in the South Atlantic convergence zone. *J. Climate,* **17,** 3829–3842, doi:10.1175/1520-0442(2004)017<3829:SVORIS>2.0.CO;2.

Liu, C., E. J. Zipser, and S. W. Nesbitt, 2007: Global distribution of tropical deep convection: Different perspectives from TRMM infrared and radar data. *J. Climate,* **20,** 489–503, doi:10.1175/JCLI4023.1.

Marengo, J. A., W. R. Soares, A. C. Saulo, and M. Nicolini, 2004: Climatology of the low-level jet east of the Andes as derived from the NCEP–NCAR reanalyses: Characteristics and temporal variability. *J. Climate,* **17,** 2261–2280, doi:10.1175/1520-0442(2004)017<2261:COTLJE>2.0.CO;2.

Monaghan, J. A., D. L. Rife, J. O. Pinto, C. A. Davis, and J. R. Hannan, 2010: Global precipitation extremes associated with diurnally varying low-level jets. *J. Climate,* **23,** 5065–5084, doi:10.1175/2010JCLI3515.1.

Nicolini, M., and A. C. Saulo, 2006: Modeled Chaco low-level jets and related precipitation patterns during the 1997–1998 warm season. *Meteor. Atmos. Phys.,* **94,** 129–143, doi:10.1007/s00703-006-0186-7.

——, and Y. García Skabar, 2011: Diurnal cycle in convergence patterns in the boundary layer east of the Andes and convection. *Atmos. Res.,* **100,** 377–390, doi:10.1016/j.atmosres.2010.09.019.

——, A. C. Saulo, J. C. Torres, and P. Salio, 2002: Strong South American low level jet events characterization during warm season and implications for enhanced precipitation. *Meteorologica,* **27,** 59–69.

——, P. Salio, G. Ulke, J. Marengo, M. Douglas, J. Paegle, and E. Zipser, 2004: South American low-level jet diurnal cycle and three-dimensional structure. *CLIVAR Exchanges,* No. 9, International CLIVAR Project Office, Southampton, United Kingdom, 6–8. [Available at http://www.clivar.org/sites/default/files/documents/Exchanges29.pdf.]

——, ——, and P. Borque, 2005: Characterization of the thermal and kinematic vertical structure of the lower troposphere in northern Argentina during SALLJEX (in Spanish). *Proc. Ninth Congreso Argentino de Meteorología,* Buenos Aires, Argentina, Centro Argentino de Meteorólogos, CD-ROM.

——, ——, and ——, 2006: Thermodynamic and kinematic characterization of the low-level troposphere during SALLJEX under different large-scale environments. *Proc. Eighth Intl. Conf. on Southern Hemisphere Meteorology and Oceanography,* Foz do Iguaçu, Brazil, Instituto Nacional de Pesquisas Espaciais, 1141–1148. [Available online at http://mtc-m15.sid.inpe.br/col/cptec.inpe.br/adm_conf/2005/10.31.19.39/doc/1141-1148.pdf.]

Nieto Ferreira, R., T. M. Rickenbach, D. L. Herdies, and L. M. V. Carvalho, 2003: Variability of South American convective cloud systems and tropospheric circulation during January–March 1998 and 1999. *Mon. Wea. Rev.,* **131,** 961–973, doi:10.1175/1520-0493(2003)131<0961:VOSACC>2.0.CO;2.

Nogués-Paegle, J., and K. C. Mo, 1997: Alternating wet and dry conditions over South America during summer. *Mon. Wea. Rev.,* **125,** 279–291, doi:10.1175/1520-0493(1997)125<0279:AWADCO>2.0.CO;2.

Paegle, J., 1998: A comparative review of South American low level jets. *Meteorologica,* **23,** 73–81.

Pielke, R. A., 2001: Influence of the spatial distribution of vegetation and soils on the prediction of cumulus convective rainfall. *Rev. Geophys.,* **39,** 151–177, doi:10.1029/1999RG000072.

Rife, D. L., J. O. Pinto, A. J. Monaghan, C. A. Davis, and J. R. Hannan, 2010: Global distribution and characteristics of diurnally varying low-level jets. *J. Climate,* **23,** 5041–5064, doi:10.1175/2010JCLI3514.1

Romatschke, U., and R. A. Houze Jr., 2010: Extreme summer convection in South America. *J. Climate,* **23,** 3761–3791, doi:10.1175/2010JCLI3465.1.

Saha, S., and Coauthors, 2010: The NCEP Climate Forecast System Reanalysis. *Bull. Amer. Meteor. Soc.,* **91,** 1015–1057, doi:10.1175/2010BAMS3001.1.

Salio, P., and M. Nicolini, 2006: Seasonal characterization of the diurnal cycle of convection frequency over southeastern South America under different low-jet conditions. *Proc. Eighth Int. Conf. on Southern Hemisphere Meteorology and Oceanography,* Foz do Iguaçu, Brazil, INPE, 24–28.

——, ——, and A. C. Saulo, 2002: Chaco low-level jet events characterization during the austral summer season. *J. Geophys. Res.,* **107,** 4816, doi:10.1029/2001JD001315.

——, ——, and E. J. Zipser, 2007: Mesoscale convective systems over southeastern South America and their relationship with the South American low-level jet. *Mon. Wea. Rev.,* **135,** 1290–1309, doi:10.1175/MWR3305.1.

Saulo, A. C., M. Nicolini, and S. C. Chou, 2000: Model characterization of the South American low-level flow during the 1997–98 spring–summer season. *Climate Dyn.,* **16,** 867–881, doi:10.1007/s003820000085.

——, M. Seluchi, and M. Nicolini, 2004: A case study of a Chaco low-level jet event. *Mon. Wea. Rev.,* **132,** 2669–2683, doi:10.1175/MWR2815.1.

——, J. Ruiz, and Y. García Skabar, 2007: Synergism between the low-level jet and organized convection at its exit region. *Mon. Wea. Rev.,* **135,** 1310–1326, doi:10.1175/MWR3317.1.

Segal, M., W. Schreiber, G. Kallos, R. A. Pielke, J. R. Garratt, J. Weaver, A. Rodi, and J. Wilson, 1989: The impact of crop areas in northeast Colorado on midsummer mesoscale thermal circulations. *Mon. Wea. Rev.,* **117,** 809–825, doi:10.1175/1520-0493(1989)117<0809:TIOCAI>2.0.CO;2.

Seluchi, M. E., and J. A. Marengo, 2000: Tropical–midlatitude exchange of air masses during summer and winter in South America: Climatic aspects and examples of intense events. *Int. J. Climatol.,* **20,** 1167–1190, doi:10.1002/1097-0088(200008)20:10<1167::AID-JOC526>3.0.CO;2-T.

——, A. C. Saulo, M. Nicolini, and P. Satyamurty, 2003: The northwestern Argentinean low: A study of two typical events. *Mon. Wea. Rev.,* **131,** 2361–2378, doi:10.1175/1520-0493(2003)131<2361:TNALAS>2.0.CO;2.

Szoke, E. J., M. L. Weisman, J. M. Brown, F. Caracena, T. W. Schlatter, 1984: A subsynoptic analysis of the Denver tornadoes of 3 June 1981. *Mon. Wea. Rev.,* **112,** 790–808, doi:10.1175/1520-0493(1984)112<0790:ASAOTD>2.0.CO;2.

Torres, J. C., 2003: Heavily precipitating mesoscale convective systems over central and northern Argentina (in Spanish). Ph.D. thesis, Facultad de Ciencias Exactas y Naturales, Universidad de Buenos Aires, Buenos Aires, Argentina, 213 pp.

Tripoli, G. J., and W. R. Cotton, 1989a: Numerical study of an observed orogenic mesoscale convective system. Part I: Simulated genesis and comparison with observations. *Mon. Wea. Rev.,* **117,** 283–304, doi:10.1175/1520-0493(1989)117<0273:NSOAOO>2.0.CO;2.

——, and ——, 1989b: Numerical study of an observed orogenic mesoscale convective system. Part II: Analysis of governing dynamics. *Mon. Wea. Rev.,* **117,** 305–328, doi:10.1175/1520-0493(1989)117<0305:NSOAOO>2.0.CO;2.

Velasco, I. Y., and J. M. Fritsch, 1987: Mesoscale convective complexes in the Americas. *J. Geophys. Res.,* **92,** 9591–9613, doi:10.1029/JD092iD08p09591.

Vera, C., and Coauthors, 2006: The South American Low-Level Jet Experiment. *Bull. Amer. Meteor. Soc.,* **87,** 63–77, doi:10.1175/BAMS-87-1-63.

Vila, D. A., 2005: Rainy mesoscale convective systems over South America: Life cycle and the associated large scale environment (in Spanish). Ph.D. thesis, Facultad de Ciencias Exactas y Naturales, Universidad de Buenos Aires, Buenos Aires, Argentina, 132 pp.

——, L. A. T. Machado, H. Laurent, and I. Velasco, 2008: Forecast and Tracking the Evolution of Cloud Clusters (ForTraCC) using satellite infrared imagery: Methodology and validation. *Wea. Forecasting,* **23,** 233–245, doi:10.1175/2007WAF2006121.1.

Whiteman, C. D., 2000: *Mountain Meteorology: Fundamentals and Applications.* Oxford University Press, 355 pp.

——, X. Bian, and S. Zhong, 1997: Low-level jet climatology from enhanced rawinsonde observations at a site in the southern Great Plains. *J. Appl. Meteor.,* **36,** 1363–1376, doi:10.1175/1520-0450(1997)036<1363:LLJCFE>2.0.CO;2.

Wilson, J. W., and W. E. Schreiber, 1986: Initiation of convective storms at radar-observed boundary-layer convergence lines. *Mon. Wea. Rev.,* **114,** 2516–2536, doi:10.1175/1520-0493(1986)114<2516:IOCSAR>2.0.CO;2.

——, and R. D. Roberts, 2006: Summary of convective storm initiation and evolution during IHOP: Observational and modeling perspective. *Mon. Wea. Rev.,* **134,** 23–47, doi:10.1175/MWR3069.1.

——, G. B. Foote, N. A. Crook, J. C. Fankhauser, C. G. Wade, J. D. Tuttle, C. Mueller, and S. K. Krueger, 1992: The role of boundary-layer convergence zones and horizontal rolls in the initiation of thunderstorms: A case study. *Mon. Wea. Rev.,* **120,** 1785–1815, doi:10.1175/1520-0493(1992)120<1785:TROBLC>2.0.CO;2.

Wolyn, P. G., and T. B. McKee, 1994: The mountain–plains circulation east of a 2-km-high north–south barrier. *Mon. Wea. Rev.,* **122,** 1490–1508, doi:10.1175/1520-0493(1994)122<1490:TMPCEO>2.0.CO;2.

Zipser, E. J., D. J. Cecil, C. Liu, S. W. Nesbitt, and D. P. Yorti, 2006: Where are the most intense thunderstorms on Earth? *Bull. Amer. Meteor. Soc.,* **87,** 1057–1071, doi:10.1175/BAMS-87-8-1057.